

The High-Temperature Oxidation Behavior of Reaction-Bonded Porous Silicon Carbide Ceramics in Dry Oxygen

Chuanwei Zheng, Zhenming Yang, and Jinsong Zhang[†]

Institute of Metal Research, Chinese Academy of Sciences, Shenyang 110016, China

The oxidation behavior of reaction-bonded porous silicon carbide (RPSC) ceramics in dry oxygen between 1100° and 1500°C was investigated based on four specimens with different porosities. RPSC ceramics exhibited a rapid mass increase in the initial stage of oxidation but a slow mass increase in the following oxidation, which was considerably different from the oxidation behavior of dense SiC. The oxidation kinetics for RPSC can be better represented by an asymptotic law rather than the parabolic law for dense SiC. We suppose that, although oxidation occurred in the entire pore channels at the beginning, the pores were rapidly blocked by the oxide as their growth rate near the pore mouth was very fast due to sufficient oxygen. As the result, the oxidation of the pore interior was stopped in the absence of further oxygen supply.

I. Introduction

Porous silicon carbide (SiC) ceramics have attracted significant attention for a number of industrial applications such as catalytic supports, hot-gas and molten metal filters, membrane supports, gas-burner media, and lightweight structural parts for elevated temperature applications.^{1–4} There are typically four methodological categories developed for manufacturing porous SiC ceramics: replication, reaction bonding, partial sintering, and expandable microspheres.⁵ Among them, the reaction bonding technique is a promising method, which involves oxidation bonding techniques,^{6–8} silicizing techniques,^{9,10} and carbothermal reduction techniques.¹¹ The reaction bonding process is characterized by a low processing temperature and a short sintering time, and is suitable for the preparation of large-size and complex-shaped components.¹² In comparison with the porous SiC prepared by other methods, reaction-bonded porous SiC (RPSC) retains its strength up to very high temperatures and has excellent thermal stability.

The chemical inertness of SiC results from the formation of a protective SiO₂ layer. Intensive investigations have been focused on the oxidation behavior of SiC materials in the form of powders,^{13,14} sintered ceramics,^{15,16} and CVD films.^{17,18} It is generally accepted that the oxidation behavior of SiC is controlled by the diffusion of oxygen molecules through the growing oxide scale as characterized by a parabolic rate model over a wide temperature range, e.g. 1100°–1500°C. A detailed review has been published by Presser and Nickel.¹⁹ Porous SiC obviously differs from dense SiC in terms of porosity and high internal surface area, which may result in a much different oxidation behavior. However, till date, a detailed study on the oxidation behavior of porous SiC is still lacking in literatures. Similar studies have been carried out on reaction-bonded Si₃N₄ (RBSN) by Porz and Thümmel,²⁰ and SiC nitride (SiCN) by Raj *et al.*²¹ In both works, the authors found that the extent of internal

oxidation of RBSN and SiCN was governed by the radius of the pore channels allowing the oxygen to penetrate the specimen. It is noticed that the RPSC contains mainly micrometer-scale open pores other than nanoscale pores like in RBSN and SiCN. It was interesting to know whether the oxidation mechanism of RBSN and SiCN can still be applied to the case of porous SiC. Moreover, the influence of porosities on the oxidation behaviors of porous ceramics has not been systematically studied. In this manuscript, we report a detailed study on the oxidation behaviors of RPSC with four different open porosities in dry oxygen and in the temperature range of 1100°–1500°C.

II. Experimental Procedure

Porous SiC materials were prepared by the reaction bonding method. In brief, aminophenolic resin, ethanol, α -SiC powder (about 6.5 μ m in size), and Si powder (about 5 μ m in size) were mixed together and then pressed at 200°C for 30 min under 20 MPa. The preforms were pyrolyzed at 800°C for 30 min, and then sintered at 1800°C for 2 h in an argon atmosphere. The resulting compacts were heated in vacuum at 1700°C to volatilize the residual silicon. Samples with a dimension of 40 mm \times 10 mm \times 4 mm were mechanically polished with 1 μ m diamond paste, followed by degreasing in acetone and ultrasonic cleaning in deionized water. RPSC materials with different porosities can be fabricated by controlling the distribution of silicon particles, pressure, and hot-pressing temperatures. For reference, dense SiC samples were also prepared by the reaction bonding method but without silicon volatilization.

Four RPSC materials with a porosity of 12.7 \pm 0.5, 17.6 \pm 0.2, 21.3 \pm 0.5, and 28.0 \pm 0.4 vol% were studied in detail, and labeled as A, B, C, and D, respectively, as shown in Table I. The bulk density (d_B) was determined by dividing the weights of the samples by their volumes. The solid density (d_s , also called skeletal density) was measured by the Archimedeian method with distilled water as the immersion medium. The open porosity was obtained from the two densities using the following equation:

$$\varepsilon = 1 - d_B/d_s \quad (1)$$

The pore volumes and volume distribution of RPSC specimens were determined with the aid of mercury porosimetry (MIP, Win9400, Micromeritics Instrument Corp., Norcross, GA). The dimension of the specimens was 10 mm \times 4 mm \times 2 mm. The diameter at 50% of the intruded mercury volume was treated as the median pore diameter. The total pore area and total intrusion volume of all RPSC materials determined by mercury porosimetry are given in Table I. The open porosity derived from the total intrusion volume is consistent with that obtained by Eq. (1). The presence of impurities in the initial samples was analyzed semiquantitatively by X-ray photoelectron spectroscopy (XPS, ESCALAB250, Thermo VG, Waltham, MA) after sputtering (for 60 s duration) with a 2 kV beam of argon ions. The results are given in Table I. No metallic silicon can be detected by X-ray diffractometry (XRD), indicating that the amount of residual silicon, if there is any, is below the detection sensitivity of the X-ray diffractometer used.

N. Jacobson—contributing editor

Manuscript No. 27000. Received October 22, 2009; approved February 3, 2010.

[†]Author to whom correspondence should be addressed. e-mail: jshzhang@imr.ac.cn

Table I. Properties of the Selected RPSC Materials

Properties	Material			
	A	B	C	D
Bulk density, d_B (g/cm ³)	2.79	2.65	2.53	2.32
Solid density, d_S (g/cm ³)	3.20	3.22	3.21	3.22
Open porosity (vol%) [†]	12.7	17.6	21.3	28.0
Median pore diameter (nm)	409	620	761	1018
Total pore area (m ² /g)	3.16	1.83	1.42	0.57
Total intrusion volume (mL/g)	0.053	0.075	0.086	0.123
Open porosity (vol%) [‡]	14.5	19.3	21.5	28.2
Impurities (wt%)				
Al		1.27		
Na		0.85		
Ca		0.50		
K		0.85		

[†]Calculated using Eq. (1). [‡]Calculated from the total intrusion volume.

The oxidation apparatus used in this work was an alumina tube furnace with MoSi₂ windings and alumina insulation. Oxygen (UHP, 99.995%) at atmospheric pressure and a flow rate of 100 standard cm³/min⁻¹ (SCCM), dried by passing through silica gel and dispersed phosphorus pentoxide desiccant towers, was used for all experiments. The oxidation temperatures were 1100–1500°C with an accuracy of ±2°C. The samples were placed in an alumina crucible and separated by SiC foam in

order to allow for free oxygen flowing. The weights of the samples (ranging from 3.4000 to 4.4000 g) were measured using an electronic balance with the sensitivity of 0.1 mg. At chosen time intervals, the sample was extracted from the furnace, cooled, weighted, and then reinserted into the furnace. In order to minimize the contamination, the alumina tube and crucible were aged under flowing oxygen for about 500 h at 1500°C before the oxidation experiments.

The morphology and composition of the samples were examined by scanning electron microscopy (SEM, S3400, Hitachi, Tokyo, Japan) and energy-dispersive spectroscopy (Inca, Oxford, Abingdon, U.K.). The crystalline phases in the samples were identified by XRD (D/max-2500PC, Rigaku, Tokyo, Japan).

III. Results and Discussion

(1) Oxidation Kinetics

The oxidation profiles of four specimens at different temperatures are plotted in Fig. 1 as a function of oxidation time. As can be seen, almost all profiles, except that for specimen D at 1400°C, are typically with a high mass increase in the initial stage but a slow mass increase in the following. This is significantly different from the oxidation behavior of dense SiC, which typically follows the linear parabolic oxidation kinetics.²² In fact, the RPSC oxidation results are better represented by an asymptotic treatment of the oxidation kinetics. Porz and Thümmel²⁰ have used an asymptotic equation to fit the oxidation of porous Si₃N₄, in which the pores were self-blocking, and the rate of oxygen transport was determined by the number of pores still remaining open. In this work, the asymptotic equation can also be adopted to represent the oxidation results of RPSC, as shown by the following equation:

$$\frac{\Delta m}{m} = \frac{\Delta m_{\infty}}{m} (1 - e^{-kat}) \quad (2)$$

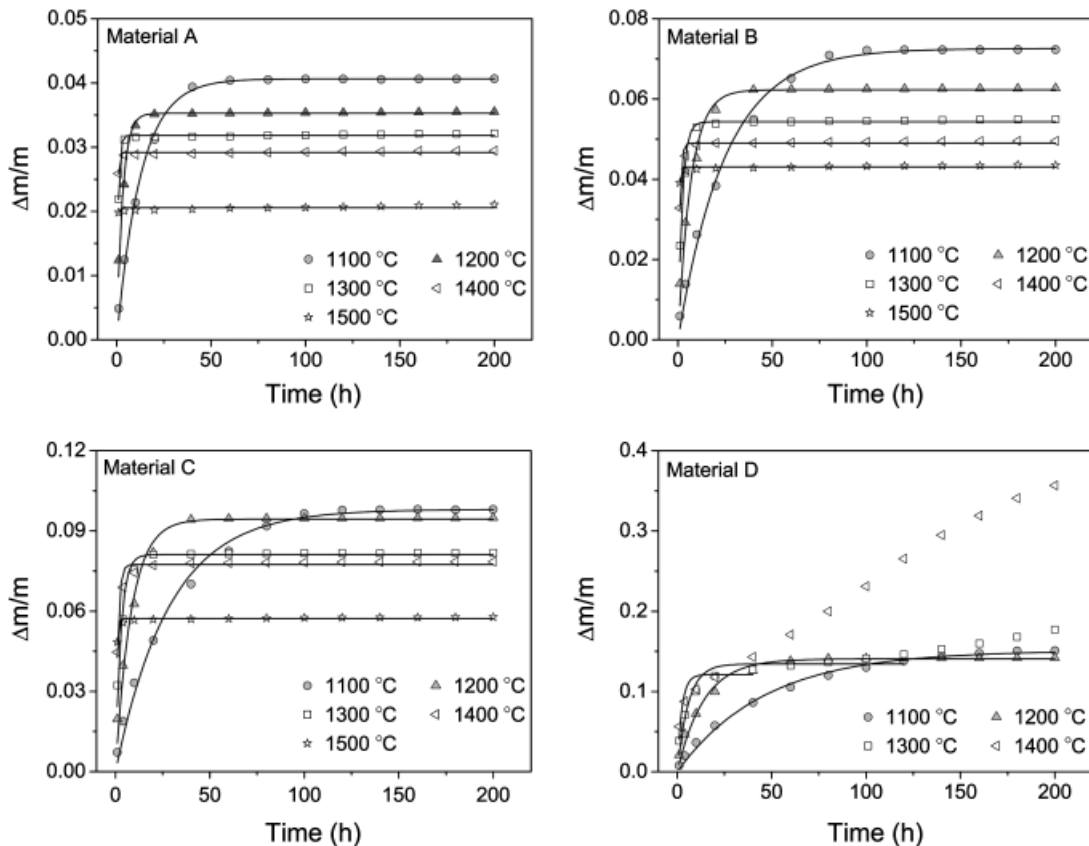


Fig. 1. Oxidation kinetics of reaction-bonded porous silicon carbide in flowing oxygen at different temperatures. The solid lines are the fitting results using the asymptotic equation.

where $\Delta m_{\infty}/m$ is the final mass gain when the horizontal region of the oxidation curve is reached and k_a is the asymptotic rate coefficient. Referring to Eq. (2), the mass gain $\Delta m/m$ can never exceed $\Delta m_{\infty}/m$. Although there is still a very low oxidation rate in the horizontal region because of the further oxidation at the external surface, this can be neglected compared with the high initial oxidation rate.

As seen from the solid lines in Fig. 1, the experimental data can be well fitted by the asymptotic Eq. (2). The fitting results for the four samples are summarized in Table II. The parameter t_{99} , representing the time by which 99% of the final mass gain was reached, was calculated using Eq. (2) and listed in Table II. We can see that the higher the oxidation temperature, the shorter the time t_{99} . In other words, the mass gain at higher temperature was lower than that at the lower temperature because of the limited time for internal oxidation for the former.

From Table II, we can also see that the $\Delta m_{\infty}/m$ and t_{99} values are extremely sensitive to the amount and type of open porosity, namely the higher porosity, the higher $\Delta m_{\infty}/m$ and t_{99} values. We believe that the higher porosity allows more oxygen to penetrate and produce more oxide. However, this silica growth results in intrinsic compressive stress in the pore channels. With enough stress being accumulated, the SiC matrix deforms and breaks, and henceforth breakaway oxidation occurs. This can be seen from Fig. 1, at 1300° and 1400°C, material D has a much higher mass gain than the fitting curves because of the breakaway oxidation.

The asymptotic rate coefficient k_a is strongly temperature dependent, as shown in Fig. 2, which plots the usual Arrhenius plot of $\ln k_a$ vs. $1/T$ (T in Kelvin). Because of the rapid change in the kinetics at 1500°C, there were no data points recorded for the early stage of the oxidation of material A. This affects the calculation of k_a and gives a very low value. The apparent activation energy (E_a) calculated from the Arrhenius plot is proportional to the open porosity, which means that the rate-controlling step of the oxidation process is correlated to the porosity.

(2) Microstructure Development

Pore-free bulk SiC materials cannot be prepared by the reaction bonding method because of the escape of organic gaseous species during the solid-state pyrolysis of polymers, which inevitably leaves a certain amount of open and closed pores. Residual silicon is also inevitable in reaction-bonded SiC. Volatilization

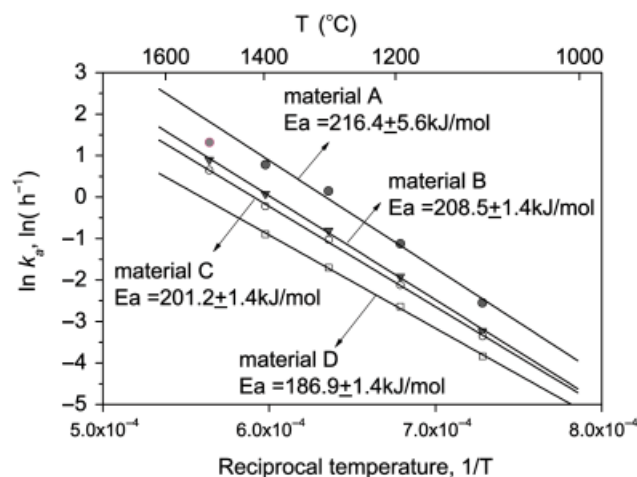


Fig. 2. Arrhenius plot of the asymptotic rate coefficients.

of this residual silicon results in micrometer- and nanometer-sized pores, which are connected to the holes created during the pyrolysis process and form open pore channels.

SEM images of material B before and after oxidation at 1200°C are shown in Fig. 3. Before oxidation, RPSC is mainly composed of SiC matrix and a mixture of micrometer- and nanometer-sized pores and associated open pore channels. Most of the pores were open and exposed to the environment, as they were created by silicon volatilization. The micrometer-sized pores were as large as 5 μm , which might be due to the micrometer-sized silicon particles used. There was a large amount of voids created after the sintering and volatilizing process. Figure 3 also shows the surface second electron image and the cross-section backscattered electron image of material B after oxidation at 1200°C for 20 (Fig. 3(c)) and 100 h (Figs. 3(d)–(f)). The surface becomes coarse and the diameters of the pores are narrowed after oxidation (see Figs. 3(c) and (d)). The cross-section image (Figs. 3(e) and (f)) shows that not only is the surface covered with an oxide layer but also the pores have been filled with SiO_2 . This means that large amounts of oxide have formed in the interior of the specimen. Oxidation of RPSC materials occurs at both the external and internal surfaces. If there is enough oxygen in the pores to support the oxidation, all of them would be completely filled with SiO_2 after a certain time. However, this is obviously not the case for our results. As seen in Figs. 3(e) and (f), there are three kinds of pores in the RPSC specimens: pores fully filled with SiO_2 (label A), pores with some annular SiO_2 (label B), and pores without SiO_2 (label C). This indicates that the oxidation in some pore channels has ceased, which will be discussed in later sections.

SEM images of material D before and after oxidation at 1300°C are shown in Fig. 4. Compared with material B, material D has a higher porosity (Fig. 4(a)), which allows more oxygen to penetrate and produces more oxide. As mentioned above, the growth of silica results in intrinsic compressive stress in the pore channels. With enough stress being accumulated, the SiC matrix deforms and breaks. This leads to breakaway oxidation, as shown in Fig. 4(b).

(3) Porosity Analysis

The porosities of four RPSC specimens before and after oxidation at 1200°C for different times, which were measured by mercury porosimetry, are shown in Fig. 5. Before oxidation, the porosities of the four materials with pore diameters larger than 2 μm were about 3 vol%. The pore diameter distribution centered at around 0.41 μm for material A, 0.62 μm for material B, 0.76 μm for material C, and 1.02 μm for material D. After oxidation, the pore channels were narrowed and the amounts of the open pores diminished with the increase of oxidation time for all four samples. For example, the pore diameter distribution

Table II. Results of Asymptotic Treatment of the Oxidation Plots

Material	Oxidation temperature (°C)	$\frac{\Delta m_{\infty}}{m}$	k_a (h^{-1})	t_{99} (h)
A	1100	0.0406 ± 0.0003	0.078 ± 0.003	58.78
	1200	0.0353 ± 0.0003	0.326 ± 0.020	14.11
	1300	0.0318 ± 0.0001	1.163 ± 0.022	3.96
	1400	0.0292 ± 0.0001	2.185 ± 0.072	2.11
	1500	0.0206 ± 0.0001	3.316 ± 0.385	1.39
B	1100	0.0726 ± 0.0007	0.040 ± 0.002	116.38
	1200	0.0623 ± 0.0006	0.147 ± 0.009	31.37
	1300	0.0543 ± 0.0005	0.446 ± 0.033	10.34
	1400	0.0490 ± 0.0002	1.083 ± 0.050	4.25
	1500	0.0431 ± 0.0001	2.381 ± 0.101	1.93
C	1100	0.0980 ± 0.0013	0.035 ± 0.002	131.95
	1200	0.0944 ± 0.0011	0.120 ± 0.008	38.33
	1300	0.0812 ± 0.0009	0.357 ± 0.030	12.89
	1400	0.0774 ± 0.0006	0.801 ± 0.056	5.75
	1500	0.0572 ± 0.0002	1.872 ± 0.067	2.46
D	1100	0.1509 ± 0.0026	0.022 ± 0.001	213.60
	1200	0.1407 ± 0.0021	0.071 ± 0.006	64.53
	1300	0.1344 ± 0.0044	0.170 ± 0.030	27.05
	1400	0.1211 ± 0.0116	0.408 ± 0.178	11.28

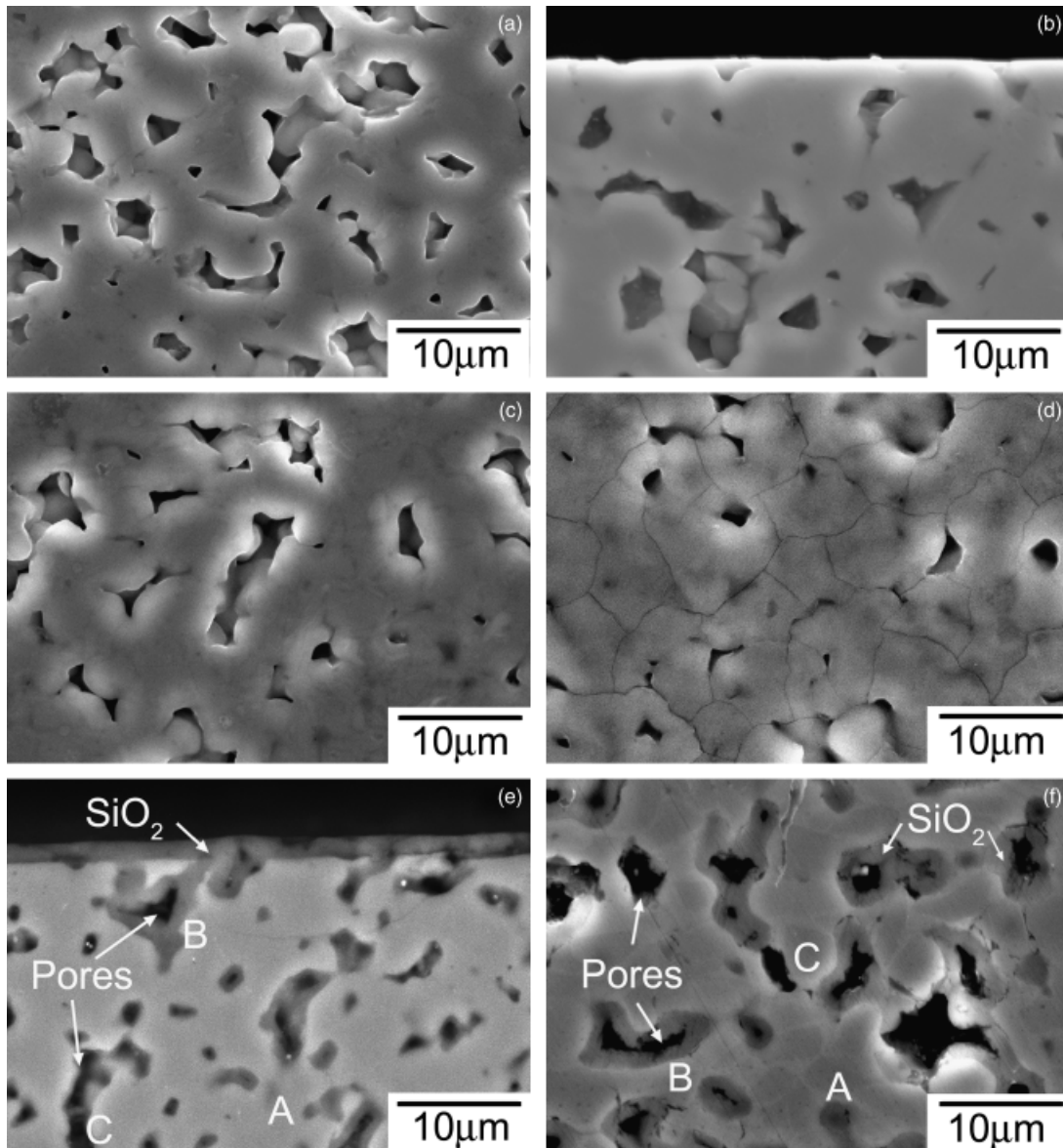


Fig. 3. Scanning electron microscopy images of surface ((a), (c), (d): SE) and cross-section ((b), (f): SE; (e): BSE) for material B before (a, b) and after oxidation at 1200°C for 20 h (c) and 100 h (d, e, f). (f) Microstructures of the cross section in the middle of the sample. SE, second electron; BSE, backscattered electron.

of material C centered at around 0.63, 0.25, and 0.04 μm after oxidation at 1200°C for 4, 20, and 40 h, respectively. Moreover, the four materials with different initial porosities show different pore distribution profiles after a certain oxidation time. For example, after oxidation for 20 h, 40% of the initial open pores are

still open and can be filled with mercury for material D. This value is 35% for material C and 31% for material B. However, for material A, only a few of the initially open pores are still open at this reaction stage. Most of them have been filled with silica. This means that the RPSC material having larger porosity

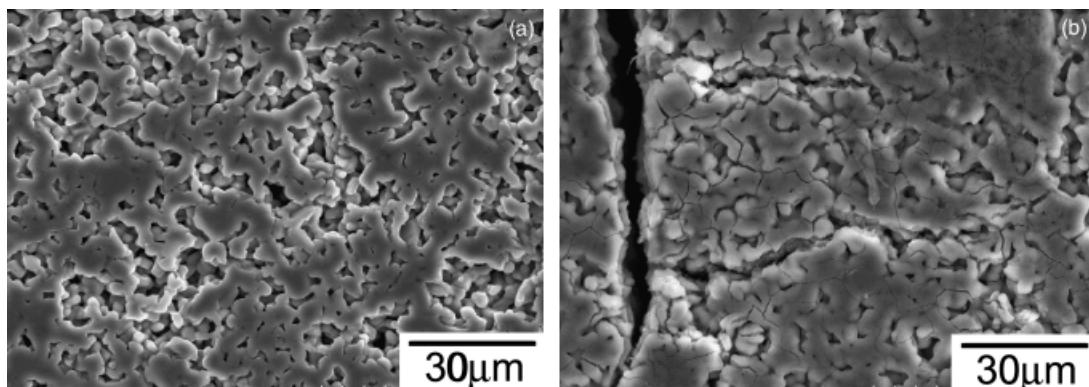


Fig. 4. Surface images of material D before (a) and after oxidized at 1300°C for 100 h. (b) A breakaway microstructure in the sample.

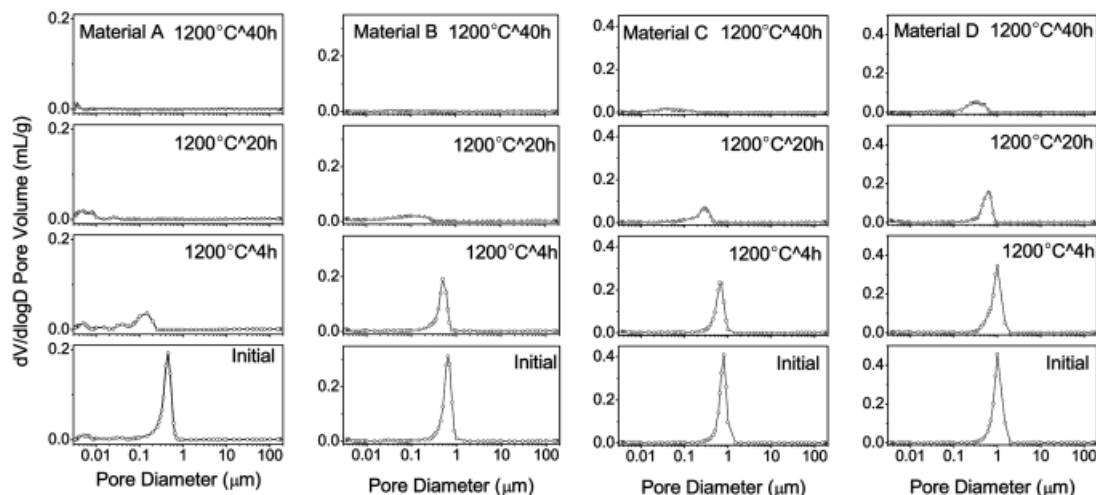


Fig. 5. Smoothed $dV/d \log D$ pore volume versus pore diameter plots for four materials before and after oxidation measured by mercury porosimetry.

needs longer time to completely fill the pores. This is consistent with the calculated t_{99} by asymptotic Eq. (2) for the materials with different starting porosities, as given in Table II.

It should be pointed out that the size of the pores obtained from the mercury porosimetry is not in agreement with that obtained from SEM observations. As illustrated in Fig. 6, the RPSC samples have micrometer-sized pores (or particle pores), nanopores, and associated open pore channels (or called “neck pores,” the “neck” part of the open pore channels that are connected to particle pores). From the mercury porosimetry, the intrusion curves give the volume that is accessible through openings to the surface greater than a certain diameter; therefore, the pore diameter distribution from the intrusion curves is not the distribution of all the pores in the entire samples, but of the open pore channels the mercury intruded. The median pore diameter is characterized to be the neck pores that are connected to internal pores.

During internal oxidation, the transport process of oxygen is similar to the intrusion process of mercury. The extent of internal oxidation of these RPSC materials is governed by the size and amount of these neck pore channels. When all the channels were completely filled with silica, the internal oxidation terminated and the horizontal region of the oxidation curve was reached.

(4) Mechanism of the RPSC Oxidation

There are five steps in the oxidation procedure: (1) diffusion of oxygen in the atmosphere to the sample, (2) inward diffusion of oxygen through the silica layer, (3) oxidation reaction at the SiC/SiO₂ interface, (4) outward diffusion of the gaseous product through the silica layer, and (5) outward diffusion of product

gases away from the surface.^{23,24} Most investigations suggest that the rate-controlling step of dense SiC oxidation would be one of (2), (3), or (4). Generally, linear kinetics of silica growth would indicate interface control mechanisms, and a parabolic time law corresponds with in- or outward diffusion-controlled processes.²⁴ However, unlike the case for dense SiC materials, the transport of molecular oxygen in the gas phase would be very important in porous SiC. The typical oxidation behavior of RPSC materials can be described as follows.

The pore channels in RPSC can be represented by a bundle of parallel cylindrical pore channels of different diameters. In one pore channel, the diffusion process of oxygen into the pore goes with the chemical reaction at the wall of the channel. As illustrated in Fig. 7, at the outer surface of the RPSC sample, there was enough oxygen to support the formation and growth of a silica layer. However, in the pore channels, the diffusion of oxygen was not fast enough to provide sufficient oxygen for the oxidation reaction with the channel wall. As the result, the oxygen concentration inside the pores was reduced gradually with the oxidation being continued. A concentration profile $c(x)$ along the pore channel has been built and shown in Fig. 7(a).²⁰ The silica layer at the channel wall was thickened in the region of the pore mouth, which reduced the open diameter of the pore channels. After a certain time, the channels were completely clogged near the mouth (Fig. 7(c)). When all the pore channels were choked, the internal oxidation terminated. The three kinds of pores labeled as A, B, and C in the cross-section image (Figs. 3(e) and (f)) were considered to correspond to the different positions in one channel (the secants marked A, B, and C in Fig. 7(c)). It is believed that a higher temperature may cause a faster growth of the silica layer near the pore mouth (Fig. 7(b)), which then leads to a quicker blocking of the pores

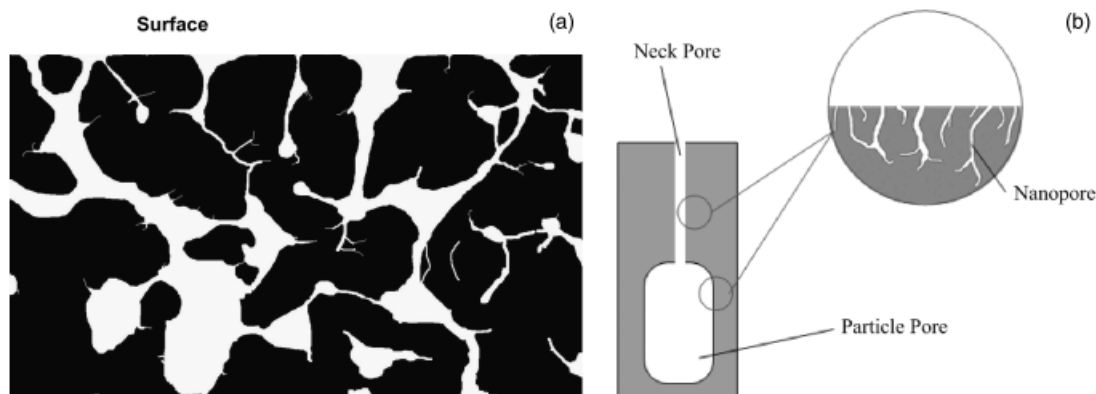


Fig. 6. Schematic illustration of a pore structure of RBSC. (a) Cross section, and (b) three kinds of pores.

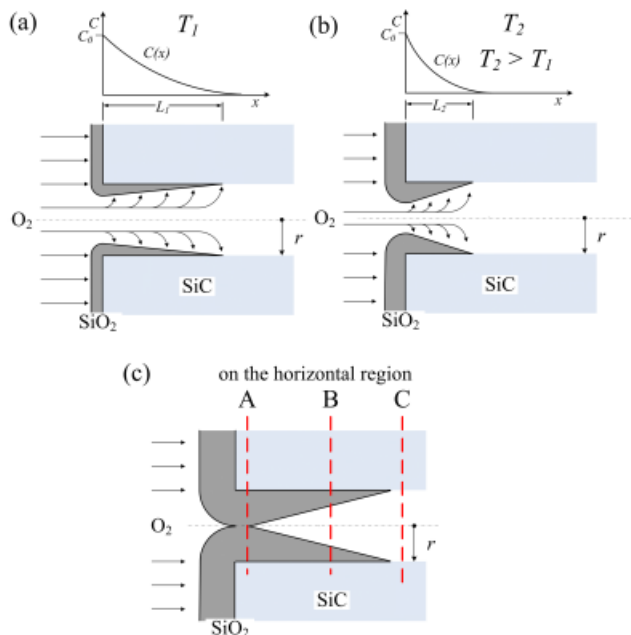


Fig. 7. Pore channel model for the internal oxidation of porous SiC.

and leaves more unoxidized regions inside the channels. This may explain why the final mass gain at higher temperatures was much lower than that at lower oxidation temperatures.

The oxidation mechanism is different in pore channels with different diameters.²¹ The pores with larger radii (r) have uniform scales throughout the length of the pores because the growth rate of oxide is slower than the rate of oxygen supply to the interior of the pores. However, when the diameters of the pore channels are extremely small, or when the pores are narrowed by silica scales, the mean free path of oxygen molecules (76 nm at room temperature but 508 nm at 1200°C) would be larger than the diameter of the channel. Under this circumstance, Knudsen flow would become effective.²⁰ The oxidation reaction is limited only to the outer part of the pore channels because of the limited possibility of oxygen diffusion into the interior of the pore channels. With the increase of temperature, the amount of oxygen is reduced rapidly because of the exponential increase of the reaction rate and only the square root dependence of Knudsen diffusivity on temperature. Pores with small diameters are easily clogged at elevated temperatures. It is believed that there must be a critical pore diameter, below which the pore mouth oxidizes fast and blocks the pore rapidly, preventing further internal oxidation. When the pores are wider than this critical pore diameter, sufficient oxygen can be transported to the pores, and the internal oxidation would proceed at the same rate as at the outer surface. In this case, the kinetics would follow the parabolic law.

IV. Conclusion

The oxidation of RPSC with porosities of 12.7, 17.6, 21.3, and 28.0 vol% has been analyzed in detail. The oxidation behavior of RPSC exhibited a typical pattern with a high initial oxidation rate, which then falls off rapidly toward longer oxidation time. In the channels of RPSC, two simultaneous processes were active: the diffusion of oxygen into the channels and the consump-

tion of oxygen by reaction with SiC to form silica. The oxide growth rate near the pore mouth was faster than the rate of oxygen supply to the interior of the pore, and thus it clogged the pore and stopped the oxidation. The oxidation of RPSC was found to be extremely sensitive to the amount and type of open porosity. Material with small pores showed good oxidation resistance. A pre-oxidation at high temperatures may limit oxygen penetration and prevent the oxidation of RPSC.

Acknowledgments

The authors thank Dr. Wensheng Zhang and Mr. Jiayuan Ye (Research Institute of Cements & New Building Materials, China Building Materials Academy) for porosity measurement. C. W. Zheng thanks Dr. Chunhai Jiang for helpful discussions.

References

- R. J. Ciora, B. Fayyaz, P. K. T. Liu, V. Suwanmethanon, R. Mallada, M. Sahimi, and T. T. Tsotsis, "Preparation and Reactive Applications of Nanoporous Silicon Carbide Membranes," *Chem. Eng. Sci.*, **59** [22–23] 4957–65 (2004).
- E. Passalacqua, S. Freni, and F. Barone, "Alkali Resistance of Tape-Cast SiC Porous Ceramic Membranes," *Mater. Lett.*, **34** [3–6] 257–62 (1998).
- X. Zhu, D. Jiang, and S. Tan, "Preparation of Silicon Carbide Reticulated Porous Ceramics," *Mater. Sci. Eng. A*, **323** [1–2] 232–8 (2002).
- L. Shi, H. Zhao, Y. Yan, and C. Tang, "Fabrication of High Purity Porous SiC Ceramics Using Coat Mix Process," *Mater. Sci. Eng. A*, **460–461**, 645–7 (2007).
- J. H. Eom, Y. W. Kim, I. H. Song, and H. D. Kim, "Microstructure and Properties of Porous Silicon Carbide Ceramics Fabricated by Carbothermal Reduction and Subsequent Sintering Process," *Mater. Sci. Eng. A*, **464** [1–2] 129–34 (2007).
- Y. S. Chun and Y. W. Kim, "Processing and Mechanical Properties of Porous Silica-Bonded Silicon Carbide Ceramics," *Met. Mater. Int.*, **11** [5] 351–5 (2005).
- J. H. She, Z. Y. Deng, J. D. Doni, and T. Ohji, "Oxidation Bonding of Porous Silicon Carbide Ceramics," *J. Mater. Sci.*, **37**, 3615–22 (2002).
- S. Liu, Y. Zeng, and D. Jiang, "Effects of CeO₂ Addition on the Properties of Cordierite-Bonded Porous SiC Ceramics," *J. Eur. Ceram. Soc.*, **29**, 1795–802 (2009).
- Y. Aoki and B. McEnaney, "SiC Foams Produced by Siliciding Carbon Foams," *Br. Ceram. Trans.*, **94** [4] 133–7 (1995).
- A. R. Maddocks and A. T. Harris, "Bioteplated Synthesis of Novel Porous SiC," *Mater. Lett.*, **63**, 748–50 (2009).
- Y. W. Kim, S. H. Kim, I. H. Song, H. D. Kim, and C. B. Park, "Fabrication of Open-Cell, Microcellular Silicon Carbide Ceramics by Carbothermal Reduction," *J. Am. Ceram. Soc.*, **88** [10] 2949–51 (2005).
- Q. Huang and Z. Jin, "The High Temperature Oxidation Behavior of Reaction-Bonded Silicon Carbide," *J. Mater. Proc. Tech.*, **110**, 142–5 (2001).
- P. J. Jorgensen, M. E. Wadsworth, and I. B. Cutler, "Oxidation of Silicon Carbide," *J. Am. Ceram. Soc.*, **64**, 613–6 (1995).
- D. Das, J. Farjas, and P. Roura, "Passive Oxidation Kinetics of SiC Microparticles," *J. Am. Ceram. Soc.*, **87** [7] 1301–5 (2004).
- J. A. Costello and R. E. Tressler, "Oxidation Kinetics of Hot-Pressed and Sintered Alpha-SiC," *J. Am. Ceram. Soc.*, **64**, 327–31 (1981).
- J. A. Costello and R. E. Tressler, "Oxidation Kinetics of Silicon Carbide Crystals and Ceramics: I, in Dry Oxygen," *J. Am. Ceram. Soc.*, **69** [9] 674–81 (1986).
- T. Narushima, T. Goto, and T. Hirai, "High Temperature Passive Oxidation of Chemically Vapor Deposited Silicon Carbide," *J. Am. Ceram. Soc.*, **72**, 1386–90 (1989).
- C. E. Ramberg, G. Cruciani, K. E. Spear, and R. E. Tressler, "Passive Oxidation Kinetics of High Purity Silicon Carbide from 800° to 1100°C," *J. Am. Ceram. Soc.*, **79**, 2897–911 (1996).
- V. Presser and K. G. Nickel, "Silica on Silicon Carbide," *Crit. Rev. Solid State Mater. Sci.*, **33** [1] 1–99 (2008).
- F. Porz and F. Thümler, "Oxidation Mechanism of Porous Silicon Nitride," *J. Mater. Sci.*, **19**, 1283–95 (1984).
- R. Raj, L. An, S. Shah, R. Riedel, C. Fasel, and H. J. Kleebe, "Oxidation Kinetics of an Amorphous Silicon Carbonitride Ceramic," *J. Am. Ceram. Soc.*, **84** [8] 1803–10 (2001).
- B. E. Deal and A. S. Grove, "General Relationship for the Thermal Oxidation of Silicon," *J. Appl. Phys.*, **36** [12] 3770–8 (1965).
- N. S. Jacobson, "Corrosion of Silicon-Based Ceramics in Combustion Environments," *J. Am. Ceram. Soc.*, **76** [1] 3–28 (1993).
- K. L. Luthra, "Some New Perspectives on Oxidation of Silicon Carbide and Silicon Nitride," *J. Am. Ceram. Soc.*, **74** [5] 1095–103 (1991). □